batteries

MDPI

Article

Untreated Natural Graphite as a Graphene Source for High-Performance Li-Ion Batteries

María Simón [1], Almudena Benítez [1], Alvaro Caballero [1,*], Julián Morales [1] and Oscar Vargas [2]

[1] Dpto. Química Inorgánica e Ingeniería Química, Instituto de Química Fina y Nanoquímica, Universidad de Córdoba, 14071 Córdoba, Spain; p12sigam@uco.es (M.S.); q62betoa@uco.es (A.B.); iq1mopaj@uco.es (J.M.)

[2] Escuela de Ingeniería Metalúrgica y Ciencia de Materiales, Universidad Industrial de Santander, Bucaramanga, Santander 680002, Colombia; osavarce@uis.edu.co

* Correspondence: alvaro.caballero@uco.es; Tel.: +34-957-21-86-20

Received: 24 January 2018; Accepted: 22 February 2018; Published: 1 March 2018

Abstract: Graphene nanosheets (GNS) are synthesized from untreated natural graphite (NG) for use as electroactive materials in Li-ion batteries (LIBs), which avoids the pollution-generating steps of purifying graphite. Through a modified Hummer method and subsequent thermal exfoliation, graphitic oxide and graphene were synthesized and characterized structurally, morphologically and chemically. Untreated natural graphite samples contain 45–50% carbon by weight; the rest is composed of different elements such as aluminium, calcium, iron, silicon and oxygen, which are present as calcium carbonate and silicates of aluminium and iron. Our results confirm that in the GO and GNS synthesized, calcium is removed due to oxidation, though other impurities are maintained because they are not affected by the synthesis. Despite the remaining mineral phases, the energy storage capacity of GNS electrodes is very promising. In addition, an electrochemical comparison between GNS and NG demonstrated that the specific capacity in GNS is higher during the whole cycling process, 770 $mA \cdot g^{-1}$ at 100th cycle, which is twice that of graphite.

Keywords: natural graphite; graphene nanosheets; Li-ion batteries

1. Introduction

The current commitment to sustainability and energy consumption presents many technical challenges, among which is the need for energy storage. The key material that can be used to address this purpose is Graphene. Graphene sheets make it possible to store Li^+ on both faces; for this reason, its theoretical energy storage capacity as electrode in Li-ion batteries is twice that of graphite [1]. Among the most studied materials in Li-ion batteries for energy storage are Graphene-based materials [2,3]. The capability of graphene in different energy devices is also being investigated deeply, such as in supercapacitors [4,5], fuel cells [6,7] and solar cells [8,9].

Chemical and physical methods can be used to isolate graphene from graphite. The most common method for producing graphene nanosheets (GNS) from graphite (natural or synthetic) is the reduction of graphene oxide (GO) obtained from graphite oxidation [10]. The synthesis of GO from graphite can be carried out using different methods based on chlorate or permanganate [11]. Today, the most commonly used technique to synthesise GO is the Hummers method, in which graphite is oxidised with $KMnO_4$ in a strongly acidic media. GO has an increased basal spacing when compared to graphite. Enlargement of the basal spacing is caused by the insertion of functional groups, mainly oxygenated groups, between the carbon layers. GO reduction can be carried out by means of chemical, electrochemical, thermal and microwave-assisted methods. The final properties of the obtained graphene depend on the raw starting material and the synthesis method [12].

Graphite is the most common source of graphene and can be classified according to its origin as natural (NG) or synthetic. Natural flake graphite is macrocrystalline and found in a greater number of mineral reserves. Nevertheless, extracting flake graphite from its surrounding minerals usually involves a complex and pollution-generating purification process due to its low abundance in ores. Vein graphite is the purest and most crystalline form found in nature, and by direct deposition of graphite, carbon from geological fluids is formed. Otherwise, synthetic graphites can be produced through the use of heat-induced graphitisation of hydrocarbon precursors. Typically, synthetic graphite can be produced in higher purity than NG [13]. However synthetic graphite has lower crystallinity than vein or natural flake graphite and is more expensive than NG. For the last few years, the price of synthetic graphite was eight times that of NG [14].

It is essential to mass-produce graphene from graphite at low cost. NG is cheaper than synthetic graphite; thus, producing graphene from untreated NG would decrease production costs. Additionally, there are huge stocks of NG minerals still in the earth. Although in the last decade NG production has grown, at current rates it is estimated that production could be maintained for over 200 years. Currently, to prepare graphene, only high-purity graphite (more than 99.9% fixed carbon) is used [15,16]. To achieve this level of purity, silicate mineral impurities in the starting graphite must be removed by vaporization at ultra-high temperature or leaching in hydrofluoric acid [17–19]. These purification techniques raise environmental concerns due to their high energy consumption or the residual fluorine in discharged waste water [20,21], respectively.

Herein, we show that untreated NG can be used to prepare high-quality graphene nanosheets that have excellent energetic properties. Si, Fe and Ca are some of the impurities that are present in NG. We demonstrate that a significant amount of these impurities still remain in the chemically reduced graphene materials although a substantial elimination is carried out during the oxidative treatment of graphite samples. Using this material as an electrode in rechargeable Li-ion batteries, the energy storage capacity was examined. Surprisingly, the impurities remaining in the sample do not affect the electrochemical properties of our electrode. Comparing these results to a similar study of synthetics samples, NG and synthesised graphene both demonstrate excellent energetic properties that surpass the energy values reported for other graphene materials obtained by similar methods from pure, synthetic graphite.

2. Materials and Methods

2.1. Synthesis of Graphene

Untreated NG from Huelma, Spain was used as a raw material. Huelma graphite is found in volcanic rocks and is an example of graphite formed from precipitation of fluids [22]. Graphite oxide (GO) was synthesized using a modification of the Hummers method [23]. In a common procedure, an aqueous solution containing 120 mL of 98% H_2SO_4 (Panreac) and 80 mL of 65% HNO_3 (Panreac) was placed in an ice-water bath and 2 g of powdered NG was added. After 20 min, the ice-water bath was removed and 10 g of $KMnO_4$ (Merck) was slowly added; the new mixture was allowed to react for 2 h, keeping the temperature at around 35 °C. A dark brown suspension was obtained and diluted with 400 mL deionised water; after adding 8.6 mL 35% H_2O_2 (Sigma-Aldrich, St. Louis, MO, USA), it turned dark yellow. Then, it was washed with 100 mL of 10% aqueous HCl (Panreac) to obtain a dark brown gel, and by washing with water and centrifuging several times, a neutral pH was achieved. Finally, GO was obtained by drying in a vacuum at 80 °C.

GNS were prepared by thermal exfoliation, heating the already-synthesized GO in a tubular oven at 300 °C for 2 h in an N_2 atmosphere at a rate of 5 °C·min^{-1}.

2.2. Sample Characterisation

A Bruker D8 Advance X-ray diffractometer was used to record X-ray diffraction (XRD) patterns, using non-monochromated Cu-Kα radiation and a graphite monochromator for the diffracted

beam. The scanning conditions for structural analysis were 5–55° (2θ), with a 0.003° step size at 12 s per step. Thermogravimetric analyses (TGA) were conducted using a Mettler Toledo under ambient conditions with a heating rate of 5 °C·min^{-1} in the presence of oxygen for NG and GNS, while GO was heated under nitrogen. Elemental analyses (EA) were carried out in an automatic LECO CHN-2000 microanalyser. JEOL JSM 6300 and JEOL JEM 1400 electronic microscopes were used to examine scanning electron microscopy (SEM) and transmission electron microscopy (TEM) images, respectively. The TEM was coupled to a microanalysis system and measured by energy-dispersive X-ray spectroscopy (EDAX). Raman measurements were carried out with a Renishaw Raman instrument (InVia Raman Microscope) equipped with a Leica microscope furnished with various lenses, monochromators and filters, in addition to a CCD. Spectra were obtained by excitation with green laser light (532 nm) from 250 to 3500 cm^{-1}. An X-ray Photoelectron Spectrometer (XPS) furnished with a Mg-K source and a chamber pressure able to reach 4×10^{-9} mbar (SPECS Phobios 150MCD) allowed us to analyse the chemical state of samples. The C 1 s line attributed to carbon, located at 284.6 eV, was used as a reference to determine binding energy values.

2.3. Electrochemical Measurements

Electrodes were prepared by mixing active material with polyvinylidinedifluoride (PVDF, Fluka) and carbon super P (Timcal) at a ratio of 80:10:10 by weight in a 1-methyl-2-pyrrolidinone (NMP, Sigma-Aldrich) solution. The slurry was coated onto a Cu foil (20 μm thickness) using the "tape-casting" technique. Electrode coating (5 mg·cm^{-2} active mass loading) was performed in 2032-type coin cells with Li metal foil as the counter and reference electrodes. The electrolyte was 1 M $LiPF_6$ dissolved in a 1:1 (*w*/*w*) mixture of ethylene carbonate (EC) and dimethyl carbonate (DMC). An Arbin BT2000 potentiostat-galvanostat system was used to perform cycling tests within a potential window of 0.01–3.0 V. Different cells were cycled at 1C, C/2, C/5 and the rate capability was tested with C (1C as the current density of 372 mA·g^{-1} for graphite and 744 mA·g^{-1} for graphene). The rate capability of the GNS was evaluated over 10 cycles at C/5, C/2 and 1C, and then again at C/2 and C/5.

3. Results and Discussion

3.1. Structural, Compositional and Morphological Characterization

The structural properties of NG, GO and GNS samples were examined by XRD technique (Figure 1). XRD patterns exhibit the characteristic peaks for all these materials. The characteristic peak of graphite appears at ca. 27° (2θ), but migrates to ca. 11° (2θ), and the lower intensity reflections disappear, when it is transformed into graphitic oxide. The complete oxidation of GO is confirmed when the graphite peak disappears. After the thermal treatment of GO, this peak moved to 2θ ~26°, which corresponds to the (002) diffraction peak of graphene because this treatment removes part of its functional groups resulting in a decrease in the interlayer spacing.

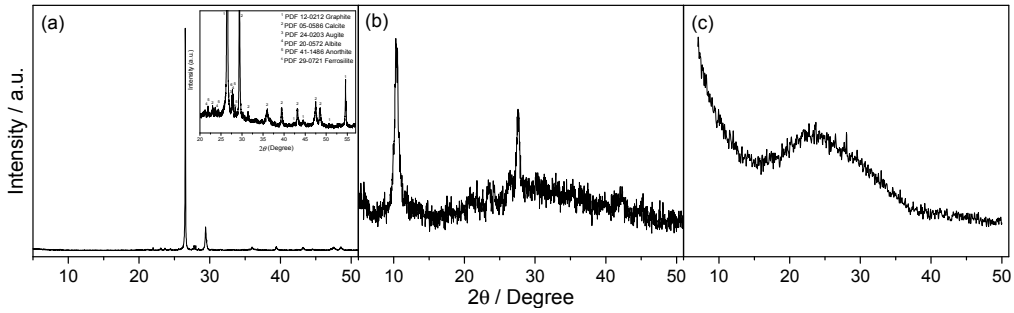

Figure 1. XRD pattern of untreated natural graphite (**a**); the inset shows the zoomed region; graphitic oxide (**b**); and graphene nanosheets (**c**).

XRD also exhibits additional peaks because of the remaining phases. NG contains calcite (05-0586 JCPDS) and aluminium and iron-based silicates with low crystallinity (in mineral phases such as augite, albite, anorthite and ferrosilite) in addition to graphite (12-0212 JCPDS). GO and GNS retain the same impurities as NG, except for calcite, which is removed during the oxidative treatment.

EDAX analysis confirms the XRD data that NG is composed of C, O, Si, Fe, Ca and Al while GO and GNS are composed of C, O, Si, Fe and Al. As expected, the calcium content of graphite disappears during oxidative treatment, which is in agreement with the XRD result. However, the Fe, Al and Si impurities are not removed by this treatment. The atomic composition values obtained from element analysis (EA) and EDAX are in agreement. Table 1 shows the EA results. Naturally, the oxygen content for GO is high, and decreases during thermal exfoliation as the temperature increases. On the other hand, during the treatment with sulfuric acid, the sulfur is incorporated and appears in the GO analysis, but decreases upon exfoliation. As discussed above with respect to XRD, the interlayer spacing tended to increase as the functional group content increased.

Table 1. Elemental analysis of samples (% ms).

Element	NG	GO	GNS
Carbon	45.73	34.78	41.84
Hydrogen	0.36	1.79	0.97
Nitrogen	0.40	0.87	1.28
Sulfur	0.01	1.63	0.98
Oxygen	13.58	37.46	19.22

The amount of each element in NG, GO and GNS was determined from TG data (Figure 2a), and values were consistent with the elemental composition analysis. The TG curve for NG obtained in an oxygen atmosphere exhibited a weight loss between 500–700 °C, which corresponds to graphite oxidation (45–50% by mass). The decarbonation of calcite occurs at slightly higher temperatures around 780–800 °C (5–10%). The rest of the sample was composed of aluminium and iron-based silicates, which are immune to the process. For unreduced GO, the main mass loss (~55%) occurred around 200 °C and is attributable to the decomposition of labile oxygen functional groups [24,25]. The mass loss at temperatures below 100 °C (~10%) can be ascribed to the removal of absorbed water, whereas the steady loss observed for higher temperatures is attributable to the release of more stable oxygen-containing functional groups [26]. The TG curve for GNS reflects its typical thermal stability up to 400 °C [27], at which point it starts to lose weight rapidly. Around 45–50% of the sample corresponds to GNS, while the rest of the sample is composed of silicates of aluminium and iron according to the other methods of analysis. The reduction process was confirmed by the absence of a mass loss around 200 °C. The TG curve of GNS also displays a significant mass loss (10%) below 100 °C due to water desorption.

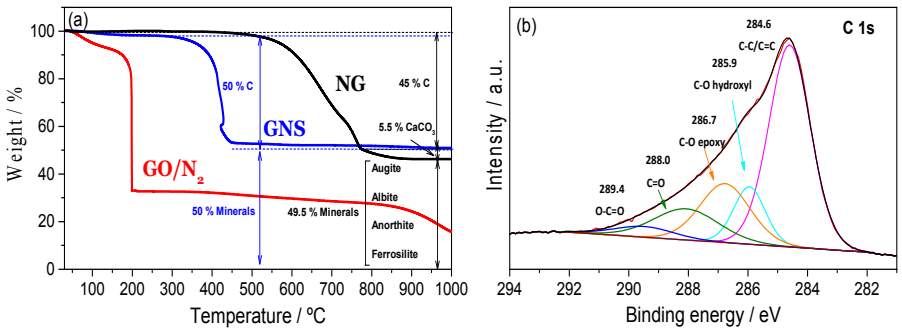

Figure 2. TG curves of NG, GO and GNS samples. The heating rate was 5 °C·min^{-1} under oxygen, except for GO, which was carried out under N_2 (**a**); XPS spectra for the C 1 s photoemission peak of the GNS sample (**b**).

In order to obtain additional information on the chemical composition, XPS spectra were obtained (Figure 2b). As expected, the C 1 s XPS spectra for GNS revealed that significant deoxygenation occurred during the thermal reduction process. The signals were well-fitted, with a combination of at least five overlapped peaks (R^2 higher than 0.999). The strongest signal at 284.6 eV was assigned to C-C bonds, while signals at 285.9, 286.7, 288.0, and 289.4 eV were assigned to oxygen-bound C in hydroxyls, epoxies, carbonyls, and carboxyl groups, respectively [28].

Raman spectroscopy is a powerful technique with which to study carbonaceous materials such as graphene, and it is also useful for examining ordered and disordered crystalline structures and distinguishing between the single and multilayer characteristics of graphene [29]. Raman spectroscopy can be used to observe the splitting of the graphite layers. The Raman spectra for NG, GO and GNS can be seen in Figure 3. The relative intensity of a couple of bands in the range 1200–1800 cm^{-1} has been proposed to be an indicator of graphene disorder [30]. The G (at ca. 1600 cm^{-1}) and D (at ca. 1350 cm^{-1}) bands are associated with the in-plane vibrational modes that involve sp^2-hybridised carbon atoms and the breathing modes of sp^2 carbon rings, respectively. The presence of defects in high-quality graphene is required for its activation [31]. The I_D/I_G ratio values increased considerably from the NG (0.14) to the GO and GNS (0.88 and 0.91 respectively), indicating that both materials possess a more defective structure and lower degree of graphitisation than natural graphite. The overlapped peaks observed for GNS (Figure 3c) in the range 2250–3300 cm^{-1} are characteristic of this carbonaceous material and suggestive of a structure consisting of stacked layers.

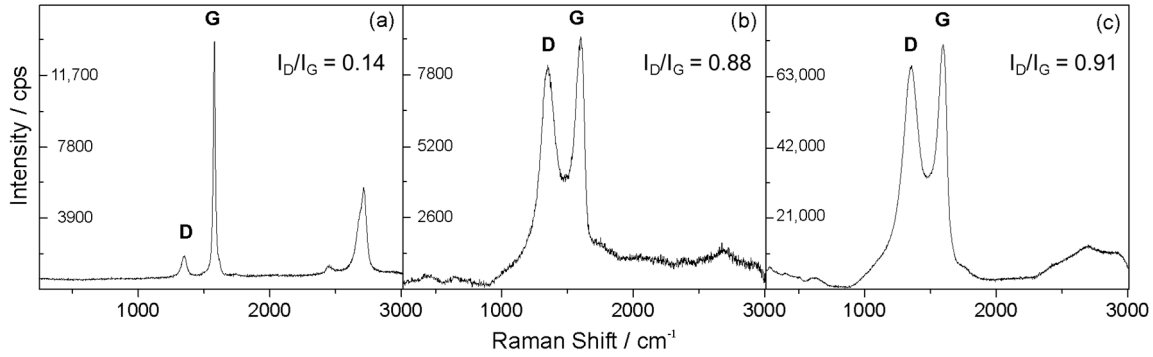

Figure 3. Raman spectra of untreated natural graphite (**a**); graphitic oxide (**b**); and graphene nanosheets (**c**).

The morphological properties of NG, GO and GNS were studied by SEM and TEM (Figure 4). Micrometric particles of graphite flakes are shown in Figure 4a. TEM images of GO and GNS samples (Figure 4b,c) contain dark and dull spots due to the mineral phases, although there are significant differences between the images. GNS exhibit the characteristic system of entangled and scrolled sheets that resemble crumpled paper. EDAX analysis of the mineral phases in the GNS sample confirmed that the graphene carbon resides in the clear area of the image while Si, Fe and Al are present in the dark spots.

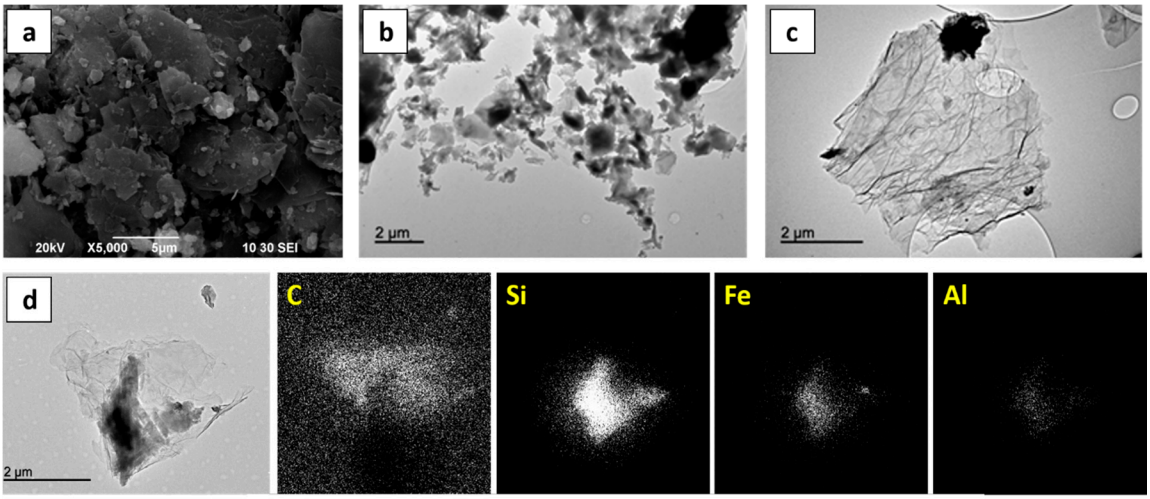

Figure 4. SEM image of NG (**a**); TEM image of GO (**b**); TEM image of GNS (**c**); EDAX mapping of C, Si, Fe and Al for a GNS sample (**d**).

3.2. Electrochemical Properties

Figure 5 shows that GNS synthesised from untreated NG have excellent energetic properties, even without using pre-lithiation strategies [32]. Figure 5a shows the discharge/charge curves for the 1st, 10th and 100th cycles of a cell made with a NG electrode while Figure 5b shows the curves of the GNS cell, both recorded at C/5. The first discharge/charge curves exhibited irreversible capacity, which is usually associated with solid electrolyte interphase (SEI) formation the origin of which can ascribed either to the silicate impurities [33] and/or to the nanoflake morphology of graphite [34]. While the initial capacity delivered for NG was 355 mA·h·g^{-1}, the capacity delivered for GNS was 1003 mA·h·g^{-1}. As expected, the GNS specific capacity in subsequent cycles was more than double the capacity of NG.

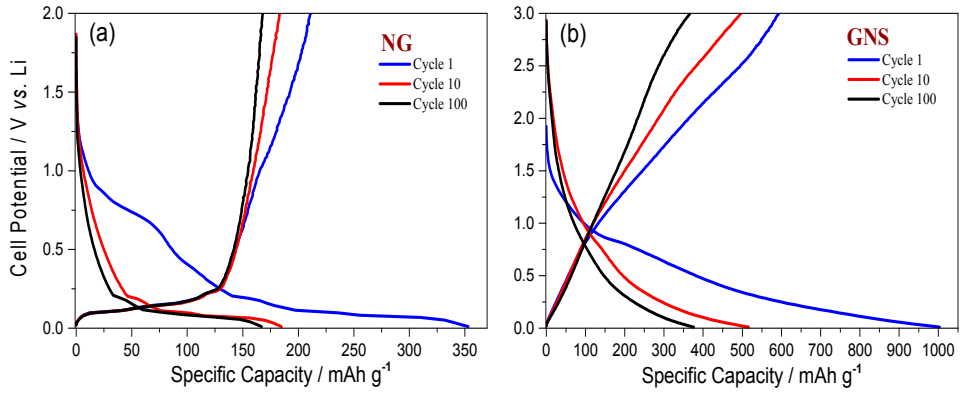

Figure 5. Discharge/charge curves for NG (**a**) and GNS electrodes (**b**) at a rate of C/5.

The capacity of these cells as a function of the number of cycles is included in Figure 6a. Both graphite and graphene exhibited a high initial irreversible capacity. As expected, the capacity retention of cells made from graphite is better than that of cells made from a GNS electrode, which is in agreement with the discharge/charge curves (Figure 5). These results are consistent with those of Hassoun et al. [35], since any chemical treatment is applied to graphite flakes. Therefore, the origin of the electrochemical irreversibility observed in real Li-ion cells could be the structural modifications of graphite flakes induced by treatment with strong chemicals for their conversion into a GNS. As a result, the charge capacity of GNS was significantly lower than its discharge capacity, at around 600

mA·h·g^{-1}. Upon further cycling, there were no remarkable modifications that affected the shape of the discharge/charge curves, and a tendency towards equalization of the specific capacities of discharge and charge was appreciable; additionally, there was an increase in the coulombic efficiency. In addition, in the first ten cycles for GNS a sharp decline in capacity was observed (Figure 6a). The capacity decreased smoothly during cycling, and the capacity retention was acceptable with an average capacity of ca. 400 mA·h·g^{-1} from the 10th cycle to the 100th. The electrodes composed of NG or synthesised graphene did not only contain carbon, so the results were corrected to determine their real electrochemical properties (Figure 6a). Only 45% of the total mass of the electrode was composed of carbon. The results show that the capacity of the GNS electrode was 770 mA·h·g^{-1}, which exceeds the theoretical capacity for graphene (744 mA·h·g^{-1}). This slight excess capacity could be provided by the conductive additive of the electrode (super P carbon), whose reversible capacity has been previously reported [36].

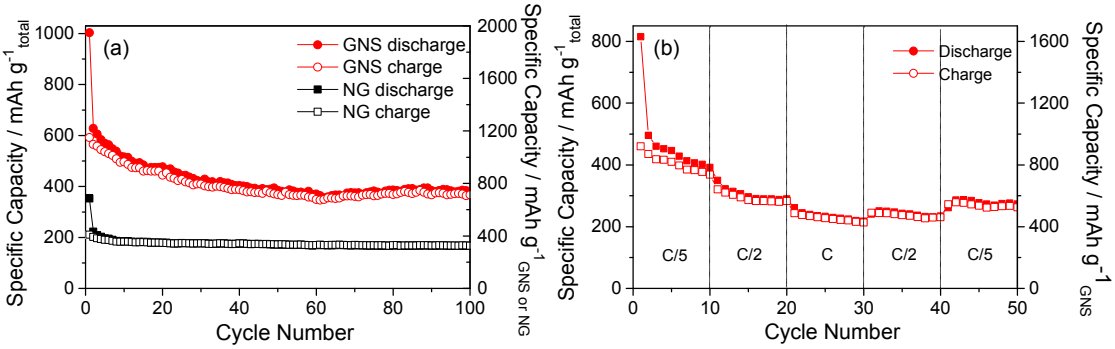

Figure 6. Cycling performance of NG and GNS electrodes at a rate of C/5 (**a**); Rate capability test of the GNS electrode (**b**).

Figure 6b shows the cyclic behaviour of GNS at different specific currents. The behaviour at C/2 and C/5 are similar, while at 1C the specific capacity is slightly lower. The electrodes delivered a high initial capacity, which then decreased and stabilised around 800 and 600 mA·h·g$^{-1}{}_{GNS}$ with cycling at C/2 and C/5. These results verify that a GNS electrode is capable of a good rate capability. It recovered the capacity delivered at a low rate after a large number of cycles irrespective of the cycling regime.

Comparing these results to similar studies with pure synthetic graphite as the graphene source [23] or graphene obtained by large-scale CVD method from acetylene [37], GNS obtained from untreated NG has excellent properties as an electrode for energy storage.

4. Conclusions

In summary, we have developed an electrode made from untreated NG for use in Li-ion batteries that has a powerful electrochemical response and exhibits a high electrochemical stability that remains constant at 200 mA·h·g^{-1} during the first 100 cycles. Additionally, we have demonstrated that it is possible to obtain graphene by the oxidation of unprocessed NG via a modified Hummer method and subsequent reduction by thermal exfoliation at 300 °C. The resulting GNS still contains impurities from the untreated NG; however, it has twice the specific capacity of NG because the remaining phases do not affect the electrochemical properties of the synthesised materials as electrodes in Li-ion batteries.

Acknowledgments: This work was performed with the financial support of the Ministerio de Economía y Competitividad (Project MAT2014-59907-R) and Junta de Andalucía (Group FQM-175).

Author Contributions: M.S. designed and performed the experiments and analyzed the results. The manuscript was written by all five authors.

Conflicts of Interest: The authors declare no conflict of interest.

References

1. Sun, Y.Q.; Wu, Q.O.; Shi, G.Q. Graphene based new energy materials. *Energy Environ. Sci.* **2011**, *4*, 1113–1132. [CrossRef]
2. Liang, M.H.; Zhi, L.J. Graphene-based electrode materials for rechargeable lithium batteries. *J. Mater. Chem.* **2009**, *19*, 5871–5878. [CrossRef]
3. Guo, F.; Silverberg, G.; Bowers, S.; Kim, S.P.; Datta, D.; Shenoy, V.; Hurt, R.H. Graphene-Based Environmental Barriers. *Environ. Sci. Technol.* **2012**, *46*, 7717–7724. [CrossRef] [PubMed]
4. Genc, R.; Alas, M.O.; Harputlu, E.; Repp, S.; Kremer, N.; Castellano, M.; Colak, S.G.; Ocakoglu, K.; Erdem, E. High-Capacitance Hybrid Supercapacitor Based on Multi-Colored Fluorescent Carbon-Dots. *Sci. Rep.* **2017**, *7*, 11222. [CrossRef] [PubMed]
5. Repp, S.; Harputlu, E.; Gurgen, S.; Castellano, M.; Kremer, N.; Pompe, N.; Worner, J.; Hoffmann, A.; Thomann, R.; Emen, F.M.; et al. Synergetic effects of Fe^{3+} doped spinel $Li_4Ti_5O_{12}$ nanoparticles on reduced graphene oxide for high surface electrode hybrid supercapacitors. *Nanoscale* **2018**, *10*, 1877–1884. [CrossRef] [PubMed]
6. He, D.; Tang, H.; Kou, Z.; Pan, M.; Sun, X.; Zhang, J.; Mu, S. Engineered Graphene Materials: Synthesis and Applications for Polymer Electrolyte Membrane Fuel Cells. *Adv. Mater.* **2017**, *29*, 1601741. [CrossRef] [PubMed]
7. Tong, X.; Wei, Q.L.; Zhan, X.X.; Zhang, G.X.; Sun, S.H. The New Graphene Family Materials: Synthesis and Applications in Oxygen Reduction Reaction. *Catalyst* **2017**, *7*, 1. [CrossRef]
8. Low, F.W.; Lai, C.W. Recent developments of graphene-TiO_2 composite nanomaterials as efficient photoelectrodes in dye-sensitized solar cells: A review. *Renew. Sustain. Energy Rev.* **2017**, *82*, 103–125. [CrossRef]
9. Eck, M.; Pham, C.V.; Züfle, S.; Neukom, M.; Sessler, M.; Scheunemann, D.; Erdem, E.; Weber, S.; Borchert, H.; Ruhstaller, B.; et al. Improved efficiency of bulk heterojunction hybrid solar cells by utilizing CdSe quantum dot–graphene nanocomposites. *Phys. Chem. Chem. Phys.* **2014**, *16*, 12251–12260. [CrossRef] [PubMed]
10. Zhu, Y.W.; Murali, S.; Cai, W.W.; Li, X.S.; Suk, J.W.; Potts, J.R.; Ruoff, R.S. Graphene and Graphene Oxide: Synthesis, Properties, and Applications. *Adv. Mater.* **2010**, *22*, 3906–3924. [CrossRef] [PubMed]
11. Hummers, W.S., Jr.; Offeman, R.E. Preparation of graphitic oxide. *J. Am. Chem. Soc.* **1958**, *80*, 1339. [CrossRef]
12. Pumera, M. Graphene-based nanomaterials for energy storage. *Energy Environ. Sci.* **2011**, *4*, 668–674. [CrossRef]
13. Pierson, H.O. *Handbook of Carbon, Graphite, Diamond and Fullerenes: Properties, Processing and Applications*; Noyes Publications: Park Ridge, NJ, USA, 1993.
14. Olson, D.W. *2010 Minerals Yearbook: Graphite*; United States Geological Survey (USGS): Reston, VA, USA, 2012; Volume 32.
15. Wu, Z.S.; Ren, W.C.; Gao, L.B.; Liu, B.L.; Jiang, C.B.; Cheng, H.M. Synthesis of high-quality graphene with a pre-determined number of layers. *Carbon* **2009**, *47*, 493–499. [CrossRef]
16. Badenhorst, H. Microstructure of natural graphite flakes revealed by oxidation: Limitations of XRD and Raman techniques for crystallinity estimates. *Carbon* **2014**, *66*, 674–690. [CrossRef]
17. Li, Y.F.; Zhu, S.F.; Wang, L. Purification of natural graphite by microwave assisted acid leaching. *Carbon* **2013**, *55*, 377–378. [CrossRef]
18. Zhang, X.-J.; Chen, B.; Gao, X.-M. Depuration of scaly graphites by high temperature graphitization. *Carbon Tech.* **2001**, *2*, 39–40.
19. Kuang, J.; Xu, H.; Xie, W.; Tang, W.; Deng, Y.; Wang, T.; Peng, S. Investigation of Purification Technology for Aphanitic Graphite by Ammonium Fluoride and Hydrochloric Acid. *Mater. Rev.* **2013**, *27*, 9–12.
20. Rao, R.B.; Patnaik, N. Preparation of high pure graphite by alkali digestion method. *Scand. J. Metall.* **2004**, *33*, 257–260. [CrossRef]
21. Cohen-Solal, M.E.; Baudoin, C.; Omouri, M.; Kuntz, D.; De Vernejoul, M.C. Bone mass in middle-aged osteoporotic men and their relatives: Familial effect. *J. Bone Miner. Res.* **1998**, *13*, 1909. [CrossRef] [PubMed]
22. Rodas, M.; Barrenechea, J.F.; Luque, F.J. Fluid-deposited graphite: The mineralization from Huelma (Jaén). *Geogaceta* **1996**, *20*, 1573.
23. Vargas, O.A.; Caballero, A.; Morales, J. Can the performance of graphene nanosheets for lithium storage in Li-ion batteries be predicted? *Nanoscale* **2012**, *4*, 2083–2092. [CrossRef] [PubMed]

24. Si, Y.; Samulski, E.T. Synthesis of water soluble graphene. *Nano Lett.* **2008**, *8*, 1679–1682. [CrossRef] [PubMed]
25. Rutter, G.M.; Crain, J.N.; Guisinger, N.P.; Li, T.; First, P.N.; Stroscio, J.A. Scattering and interference in epitaxial graphene. *Science* **2007**, *317*, 219–222. [CrossRef] [PubMed]
26. Paredes, J.I.; Villar-Rodil, S.; Martinez-Alonso, A.; Tascon, J.M.D. Graphene oxide dispersions in organic solvents. *Langmuir* **2008**, *24*, 10560–10564. [CrossRef] [PubMed]
27. Wu, Z.S.; Ren, W.C.; Xu, L.; Li, F.; Cheng, H.M. Doped Graphene Sheets As Anode Materials with Superhigh Rate and Large Capacity for Lithium Ion Batteries. *ACS Nano* **2011**, *5*, 5463–5471. [CrossRef] [PubMed]
28. Abouimrane, A.; Compton, O.C.; Amine, K.; Nguyen, S.T. Non-Annealed Graphene Paper as a Binder-Free Anode for Lithium-Ion Batteries. *J. Phys. Chem. C* **2010**, *114*, 12800–12804. [CrossRef]
29. Guo, H.L.; Wang, X.F.; Qian, Q.Y.; Wang, F.B.; Xia, X.H. A Green Approach to the Synthesis of Graphene Nanosheets. *ACS Nano* **2009**, *3*, 2653–2659. [CrossRef] [PubMed]
30. Ni, Z.H.; Wang, Y.Y.; Yu, T.; Shen, Z.X. Raman Spectroscopy and Imaging of Graphene. *Nano Res.* **2008**, *1*, 273–291. [CrossRef]
31. Pimenta, M.A.; Dresselhaus, G.; Dresselhaus, M.S.; Cancado, L.G.; Jorio, A.; Saito, R. Studying disorder in graphite-based systems by Raman spectroscopy. *Phys. Chem. Chem. Phys.* **2007**, *9*, 1276–1291. [CrossRef] [PubMed]
32. Holtstiege, F.; Bärmann, P.; Nölle, R.; Winter, M.; Placke, T. Pre-Lithiation Strategies for Rechargeable Energy Storage Technologies: Concepts, Promises and Challenges. *Batteries* **2018**, *4*, 4. [CrossRef]
33. Yang, J.; Guo, Y.Y.; Zhang, Y.F.; Sun, C.C.; Yan, Q.Y.; Dong, X.C. Cobalt silicate hierarchical hollow spheres for lithium-ion batteries. *Nanotechnology* **2016**, *27*, 7. [CrossRef] [PubMed]
34. Arrebola, J.C.; Caballero, A.; Hernan, L.; Morales, J. Graphitized Carbons of Variable Morphology and Crystallinity: A Comparative Study of Their Performance in Lithium Cells. *J. Electrochem. Soc.* **2009**, *156*, A986–A992. [CrossRef]
35. Hassoun, J.; Bonaccorso, F.; Agostini, M.; Angelucci, M.; Betti, M.G.; Cingolani, R.; Gemmi, M.; Mariani, C.; Panero, S.; Pellegrini, V.; et al. An Advanced Lithium-Ion Battery Based on a Graphene Anode and a Lithium Iron Phosphate Cathode. *Nano Lett.* **2014**, *14*, 4901–4906. [CrossRef] [PubMed]
36. Peng, B.; Xu, Y.; Wang, X.; Shi, X.; Mulder, F.M. The electrochemical performance of super P carbon black in reversible Li/Na ion uptake. *Sci. China Phys. Mech. Astron.* **2017**, *60*, 064611. [CrossRef]
37. Chen, S.; Bao, P.; Xiao, L.; Wang, G. Large-scale and low cost synthesis of graphene as high capacity anode materials for lithium-ion batteries. *Carbon* **2013**, *64*, 158–169. [CrossRef]